Corner Detection in Images under Different Noise Levels

Yi Song*, Yiping Shen*, Shuxiao Li*, Chengfei Zhu*, Jinglan Zhang†, Hongxing Chang*
*The Integrated Information System Research Center
Institute of Automation, Chinese Academy of Sciences, Beijing, China
†Queensland University of Technology, Brisbane, Australia

***Abstract*—Corner detection has shown its great importance in many computer vision tasks. However, in real-world applications, noise in the image strongly affects the performance of corner detectors. Few corner detectors have been designed to be robust to heavy noise by now, partly because the noise could be reduced by a denoising procedure. In this paper, we present a corner detector that could find discriminative corners in images contaminated by noise of different levels, without any denoising procedure. Candidate corners (i.e., features) are firstly detected by a modified SUSAN approach, and then false corners in noise are rejected based on their local characteristics. Features in flat regions are removed based on their intensity centroid, and features on edge structures are removed using the Harris response. The detector is self-adaptive to noise since the image signal-to-noise ratio (SNR) is automatically estimated to choose an appropriate threshold for refining features. Experimental results show that our detector has better performance at locating discriminative corners in images with strong noise than other widely used corner or keypoint detectors.**

***Keywords*-corner detector; noisy image; signal-to-noise ratio; feature detection**

I. Introduction

In the field of computer vision, local invariant point features, including corners, play a significant role in the base of intellective vision tasks such as object detection and recognition [1], [2], visual tracking [3], and image retrieval [4]. For this reason, a robust corner detector is of great importance.

In real computer vision applications, we face a challenge of dealing with noisy images. For example, videos captured from the surveillance cameras are heavily contaminated by electronic noise, either from the sensors or from the circuitry of the capture devices [5]. Another example is the embedded applications of image processing tasks, where microcontrollers (MCUs) or digital signal processors (DSPs) are used for processing the images. In this case, the distraction of electronic noise could be very large during the image capturing, resulting in images with high level noise. Few corner detectors have been designed to be robust to heavy noise by now, partly because the noise could be reduced by a denoising procedure. However, noise in the image could not be removed entirely by any denoising procedure, and details of the image would also be lost as the consequence. On the contrary, if we abandon these denoising procedures, a large number of features are falsely detected in noisy images, which generates unnecessary burden for higher level processing in the vision system.

Numerous local feature detectors have been proposed. Harris detector [6] measures the self-similarity of an image patch by computing a local sum-of-squared-difference matrix, and locates corners where its self-similarity is low in all directions. SUSAN [7] calculates the proportion of the similar-to-nucleus pixels in a circular mask centered on the nucleus, and locates the local minima as corners. SIFT [1] convolves the image with a difference-of-Gaussian (DoG) kernel at various scales to generate the difference-of-Gaussian images, and detects scale-invariant keypoints by selecting local extrema in both space and scale. FAST and its variants [8] test the contiguous number of brighter or darker pixels in a ring around the center pixel to find corners, and accelerates the computation using machine learning. These approaches have been widely studied, but their performance in noisy images is rarely focused.

Noise level, which can be measured by noise variance, noise standard deviation, or signal-to-noise ratio (SNR), is an important parameter for algorithms applied to image denoising [9], segmentation [10] and registration [11]. Pyatykh *et al.* [12] extract image blocks whose presented vectors lie in the subspace of the full dimension space, and apply Principal Component Analysis (PCA) to the vectors for estimating the noise variance. Zoran & Weiss [13] assume that the kurtosis of the marginal bandpass filter response distributions remains constant throughout scales, and estimate the noise standard deviation by optimizing the parameters in their model based on the assumption. As for SNR estimation, Thong *et al.* [14] estimate the value of noise-free image autocorrelation from the offset of noisy image autocorrelation, and use it to calculate image SNR by reconstructing the formula which Frank & Al-Ali proposed in [15]. Zou [16] proposes to calculate local variances throughout the image to estimate the variance of the signal and the noise, and gets the estimated SNR by the direct ratio of the two values, with a rectification. All of the above approaches deal with the whole image to get an accurate estimation of noise level, which spends excessive time for a corner detector. In contrast, our approach sacrifices a little accuracy of the estimated SNR to obtain computational efficiency for corner detection.

In this paper, we focus on the performance of corner detectors in noisy images, and propose an improved corner detector that could find discriminative corners in images under different noise levels, without any denoising procedure. Our main contributions are:

- A modified SUSAN [7] corner detector which locates corners more accurately in noise-free images

than SUSAN.

- Two simple strategies for rejecting false corners detected in noisy images.
- An efficient method for image SNR estimation, which is embedded to the corner detector.
- A learning algorithm for obtaining a good threshold of Harris response to reject false corners on edge structures with respect to different noise levels.

Note that we only deal with the signal-independent additive white Gaussian noise (AWGN) in this paper, since it is most widely used [12].

II. Candidate Corner Detector

SUSAN corner detector has the ability to detect corners in noisy images, since the algorithm do not compute image derivatives. However, in real images, a large number of corners are detected on edge structures by SUSAN. In our detector, a small change of the principle in SUSAN detector is made to solve the problem. For a circular mask centered on a pixel *O*, we first give a label to any pixel *r* except *O* within the mask by the following rule:

$$S_r = \begin{cases} d, & I_r < I_O - t \quad (darker) \\ s, & I_O - t \le I_r \le I_O + t \quad (similar) \\ b, & I_O + t < I_r \quad (brighter) \end{cases} \tag{1}$$

where I_O is the brightness of the center pixel, I_r is the brightness of the pixel *r*, *t* is a predefined threshold. Then, we separate the pixels into two sets C_D and C_B, with $C_D = \{r | S_r = d \ or \ S_r = s\}$ and $C_B = \{r | S_r = b \ or \ S_r = s\}$, and choose the one with fewer number of pixels to be the dark-or-bright region (DOBR). The center pixel is likely to be a corner if the area of the DOBR is smaller than half of the mask area, which means the spanned angle is smaller than π. Let N_c denote the area of the DOBR, S denote that of the mask, then the corner response R_c is calculated by:

$$R_c = \begin{cases} \frac{1}{4}S - \left| N_c - \frac{1}{4}S \right|, & n_1 \le N_c \le n_2 \\ 0, & otherwise \end{cases} \tag{2}$$

where n_1 and n_2 are constants that restrict the angle of the corner to be detected. In our implementation, the same circular mask as in SUSAN approach is used, where *S* equals to 36 with the radius *R* of 3.4. We set $n_1 = 2, n_2 = 16$ to obtain corners with their angles ranging from $[\pi/9, 8\pi/9]$.

Surely a restriction should be added to confirm corners, since the algorithm could not tell if the DOBR is compact or not. We propose to use a geometric constraint in [17]. A feature with its circular mask centered on a pixel *O* is illustrated in Fig. 1, with a radius of *R*. Let *G* denote the centroid of the DOBR, β denote the angle spanned by the DOBR, then the following equation is obtained:

$$d_{OG} = \sqrt{x_{OG}^2 + y_{OG}^2} = \frac{4R \sin \frac{\beta}{2}}{3\beta} \tag{3}$$

where $\beta = \frac{2\pi N_c}{S}$. Given the coordinates of the pixels in DOBR, we can calculate the left side of Equ. (3); given R and N_c, we can calculate the right side of it. If these two results are equal, the DOBR of the feature is compact. In our implementation, we accept the feature as a corner if the absolute value of the difference of the two results is smaller than a threshold T_i (set to be a small value of 1), as the mask used for detection is not ideally circular and the corner in digital images does not have an ideal angle.

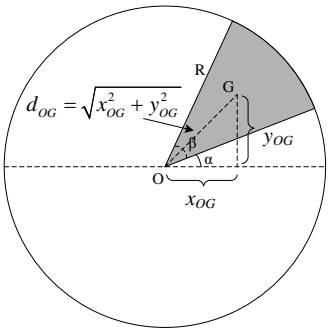

Figure 1: The circular mask centered on O. The DOBR is showed as the dark part of the mask, and G denotes the centroid of it.

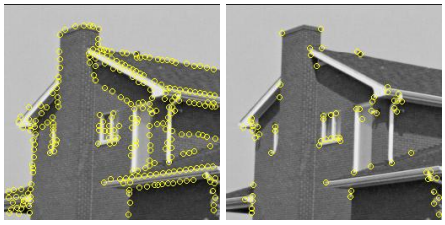

(a) (b)

Figure 2: Corners detected by (a) SUSAN (b) GDOBR in *house* image. A 7×7 mask is used for nonmaximal suppression.

As shown in Fig. 2, SUSAN detects a large number of features on edge structures in the noise-free image, while the proposed approach does not. We call our method GDOBR since it finds corners by calculating the Geometrically restricted DOBR area. With its simple computation, GDOBR is much faster than Harris or DoG detector. Since the area of DOBR is computed, a small change of the brightness within the mask yield little effect in locating corners, which makes GDOBR less sensitive to noise than FAST detector.

III. Refine Features in Noisy Images

Generally, in noisy images, corners detected by GDOBR have two kinds of false positives: (1) features in flat regions of the image are labeled as corners; (2) features on edge structures are detected as corners. In this section, we describe how our method solves these problems to obtain robust corners in noisy images.

A. Reject False Corners in Flat Regions

As for the features detected in homogeneous regions of the image, we use a simple measure referring to the intensity centroid [18] to reject them. For an image patch, the moments are defined as:

$$m_{pq} = \sum_{x,y} x^p y^q I(x, y) \tag{4}$$

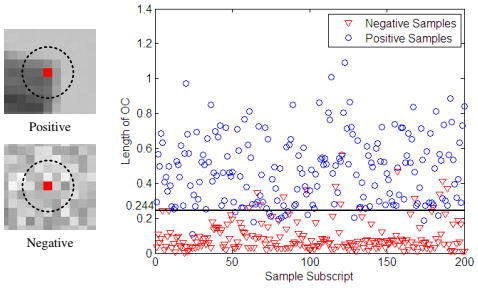

Figure 3: Feature samples used for training and their corresponding *OC* lengths. In the left images, the red pixel indicates the center pixel of the features, and the dotted circle indicates the boundary of the mask. The black line in the right image indicates the optimal value of T_c.

then the coordinates of the intensity centroid is computed by $C = \left(\frac{m_{10}}{m_{00}}, \frac{m_{01}}{m_{00}}\right)$. We utilize the modulus of the vector from the center pixel *O* to the centroid *C*, $|\overrightarrow{OC}|$, which indicates the length of *OC*, to reject false corners. In our algorithm, the moments are computed within the circular mask of radius *R* around the center pixel, so that *x* and *y* range from [-*R*, *R*].

As the added noise is pixel independent, the pixels in the mask would be uniformly affected by the noise. Therefore, if a feature in flat regions of the image is labeled as a corner, its intensity centroid *C* will locate near the center pixel *O*, thus the corners should be rejected where $|\overrightarrow{OC}|$ is smaller than a threshold T_c. We trained for T_c using 200 negative feature samples and 200 positive ones. Features detected by GDOBR in flat regions of noisy images were labeled as negative samples, and those detected on real corners in both noisy images and noise-free images were labeled as positive ones. Fig. 3 shows the training results, with T_c = 0.244 yielding the minimum loss.

After the intensity centroid measurement is done, the features detected by GDOBR are divided into two groups: "negative" and "positive". The "negative" features are the features rejected by the measurement and assumed to be located in flat regions of the image, and the "positive" ones are those accepted by the measurement. The features in the two groups are then utilized to estimate the image SNR, which will be described in the next subsection.

B. Reject False Corners on Edge Structures

Features located on edge structures are unstable. We find that Harris corner response [6] is a good way to reject these features also in noisy images. For each detected feature, its Harris response R_H is calculated within the detection mask, with the intensity value normalized. A feature is accepted as a corner if its R_H exceeds a threshold T_H.

An ideal T_H should eliminate all the false corners on edge structures and maintain discriminative corners meanwhile, but it changes with the strength of noise. Thus, we develop a learning algorithm for the detector to automatically choose an appropriate T_H for images with noise of different levels. In the following, we first introduce our method of the SNR estimation, and then describe the learning algorithm.

Estimating image signal-to-noise ratio. Noise level should be estimated for automatically choosing the best T_H. Here we use SNR as the measurement of the noise level. For a noisy image, the image SNR can be estimated by the ratio of the signal variance to the noise variance as Zou describes in [16], and the decibel formation is:

$$SNR(dB) = 10\log_{10}\frac{P_s}{P_n} \approx 10\log_{10}\frac{\sigma_s^2}{\sigma_n^2} \tag{5}$$

The signal variance could not be obtained directly since an image could not be treated as a stationary stochastic process with independent and identically distributed variables. Zou [16] proposes to use image patch variance to roughly obtain these two variances from the noisy image. For an image patch *P*, its variance refers to the intensity variance computed by all the pixels within:

$$\sigma_P^2 = \frac{1}{N}\sum_{x,y}\left[I(x,y) - \mu_P\right]^2 \tag{6}$$

where *N* denotes the number of pixels in *P*, and μ_P refers to the mean intensity of all the pixels in *P*. In Zou's method, the two variances are estimated by calculating all the patch variances in the image, while our method makes use of the detected features to do the estimation.

As mentioned in section III-A, the intensity centroid measurement has divided the detected features into "negative" and "positive" ones. N_1 "negative" features and N_2 "positive" features are used to estimate the noise variance and the signal variance, respectively. The minimum value of the variances of the patches centered on "negative" features is calculated as σ_{min}^2, as the noise variance. The maximum value of the variances of the patches centered on "positive" features is calculated as σ_{max}^2, as the signal variance. Again, the detection mask is used as the image patch. In the case that none of the detected features are located in flat regions (and this is always the case when image noise level is low), σ_{min}^2 is not a good estimation of the noise variance. To solve this problem, we randomly choose N_r patches in the image and calculate their variances. Assuming that these variances are ranging from σ_1^2 to σ_2^2, then the maximum of σ_{max}^2 and σ_2^2 is the estimation of signal variance σ_s^2, while the minimum of σ_{min}^2 and σ_1^2 is the estimation of noise variance σ_n^2, and SNR is computed by Equ. (5). Larger N_1, N_2, and N_r may generate more accurate results, but at a cost of higher computation. In our implementation, N_1 and N_2 are both set to be 20, and N_r is set to be 16.

We investigated that this estimated SNR should be normalized by the mean value of the variances of the patches centered on "positive" features, since the estimated signal variance is "enlarged" considering the effect of noise. Therefore, the equation for SNR estimation becomes:

$$SNR_{est}(dB) = 10\log_{10}\left(\frac{C}{\frac{1}{N_2}\sum_i \sigma_i^2}\cdot\frac{\sigma_s^2}{\sigma_n^2}\right) \tag{7}$$

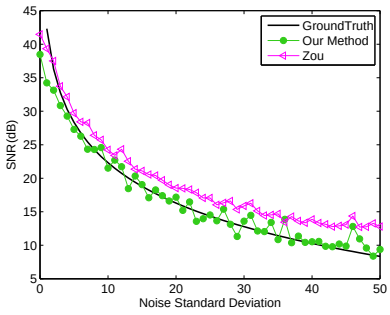

Figure 4: SNR estimation results on noisy $house$ images. The $house$ image is added by zero-mean Gaussian noise with the standard deviation ranges from 1 to 50. The groundtruth is the true value of image SNR.

where C is a trivial constant which only determines the offset of the estimated SNR values. Note that our method obtains a rough estimation for image SNR. For corner detection, limited computing time restricts the accuracy of SNR estimation. Besides, a rough estimated value is enough to obtain an appropriate T_H for further processing.

We tested our method in noisy $house$ images, compared with Zou's. Fig. 4 illustrates that our method gives a good estimation for noise levels, in spite of some fluctuations.

Learning for Optimal T_H. A learning algorithm is developed for the detector to choose an appropriate T_H. First we set up a database composed of noise-free images, then noise of different strengths is added to each image to produce a series of noisy images. Thus image groups are generated, with each group containing a noise-free image and its noisy images. The learning procedure is:

1) For the noise-free image in each group, detect features using GDOBR. Refine the features and estimate the image SNR. A fixed T_H denoted by T_{H0} is given to the refining.
2) For noisy images in the same group, do the same detection process. For each image, search for the T_H that yields the highest *F1* score (described in section IV-A) comparing with the noise-free image and record the corresponding SNR estimated in the detection.
3) Get all the pairs of the optimal T_H (including T_{H0}) and its corresponding SNR. Fit the curve of T_H in terms of SNR, making the fit error minimized.

The key of this algorithm is the curve fitting process for the optimal T_H, which can be described as to find a continuous function that satisfies:

$$\begin{aligned} \widehat{f}(x) &= \arg\min_{f(x)} \|T - f(x)\| \\ s.t. \quad & f(x) > 0, \forall x \end{aligned} \tag{8}$$

where $\|\cdot\|$ is the standard L_2 norm in the Euclidean space.

The model is too hard to be solved because the model function could be arbitrary, but with a given function type we may find the solution efficiently. Details of the algorithm are presented in section IV-B.

IV. Experimental Results and Evaluations

A. Evaluation Criterion

The performance of point feature detectors can be treated as a point matching problem, and the *F1 score* is used for evaluation. For an image pair, a feature is a "repeated" feature if it is detected in both images. The precision Pre and recall Rec can be defined as follows:

$$Pre = \frac{\text{number of } repeated\ features}{\text{number of } detected\ features} \tag{9}$$

$$Rec = \frac{\text{number of } repeated\ features}{\text{number of } potential\ features} \tag{10}$$

where the "detected features" is the features which are detected in the second image and appear in the region of the first image; the "potential features" is the features which are detected in the first image and can potentially be detected in the second image. Then, the *F1 score* is defined as $F_1 = \frac{2 \cdot Pre \cdot Rec}{Pre + Rec}$, which measures the performance of repeatability with respect to both images.

B. Process of the Learning

The learning algorithm for choosing optimal T_H is significantly important since the learning result determines the noise adaptability of our detector. Details in the algorithm are as follows. The noise-free images are 26 gray images with the size of 378×251 pixels from Caltech Background image dataset [19]. Zero-mean Gaussian noise with standard deviation from 1 to 50 is added to each image, generating 1300 noisy images for training. Since we mainly train for optimal T_H, some other parameters are empirically set. The brightness threshold t is set to be 15 and remains unchanged through the whole processing. For the noise-free images, T_{H0} is set to be a small value of 0.04 to maintain discriminative corners. On estimating SNR, the constant C is fixed as 4088 since it performs well for these images. For each noisy image, the optimal T_H is searched from 0.01 to 3, with the step of 0.01.

Values of the optimal T_H in terms of estimated SNR, and the results of the fitting curves are shown in Fig. 5. Functions of three types are used to fit the values in our experiments, which are exponential function, multi-Gaussian function and piecewise linear function. Formations and the parameters of the best fitting of each type are listed in Table II, where RMSE means the root mean squared error of the fitting curves. Piecewise linear fitting yields the smallest RMSE among the three functions.

C. Performance Evaluation and Discussion

In order to validate our detection approach, we ran sufficient experiments on establishing our detector. Also, we compared our approach with other commonly used point feature detectors on performance in noisy images.

A brief comparison on speed of GDOBR and other detectors in noise-free images is shown in Table I. The experiment is set up on a PC with a 2GHz Intel Core2 processer, and 51 gray images sized 378×251 from the Background dataset are used for the test. Corner detection is run 10 times for each image and the average time cost

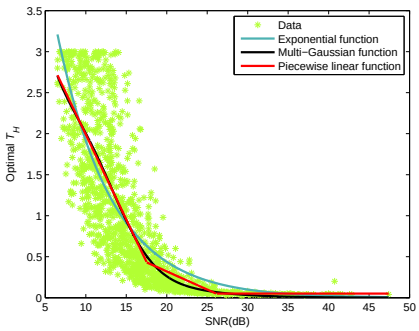

Figure 5: Results of the best fitting curves for three types of functions.

Detector	FAST-9	GDOBR	SUSAN	Harris	DoG
Time per image (ms)	1.393	7.216	29.955	60.580	351.071

Table I: Average time cost of different detectors

per image is obtained. The results show that GDOBR is faster than all the other detectors except FAST-9 which is accelerated by machine learning.

Fig. 6 shows the detection results in noisy images at different stages of our algorithm. Numerous corners are located in flat regions and on edge structures using GDOBR in noisy images. False corners in flat regions are rejected by measuring the intensity centroid, and false corners on edge structures are further rejected after thresholding Harris response of the corners with the adaptive threshold based on SNR.

We have applied the three best fitting functions to our detection approach and compared their performance against other detectors in images under different noise levels. Another 25 gray images (except those used for learning) sized 378×251 from the Background dataset and those added with noise are used for the test. First the corner detection is applied to the noise-free images and their corresponding noisy images, then the *F1* score is obtained by comparing the detected corners in the noise-free image with those in the noisy images. For SUSAN detector, we use the standard implementation in [20]. For DoG detector [1], we use the initial smoothing blur of value 1 to yield robust results in different noise levels. For others, feature numbers are controlled about the same by thresholding on the response of detected corners in noise-free images, with an average number of 240. A 7×7 mask is applied to accomplish nonmaximal suppression for all detectors except FAST-9, which uses a 3×3 mask [8].

Details of the performance are shown in Fig. 7. We name our three detection approaches by the name of fitting functions for short. Both of FAST-9 and Harris detectors yield high *F1* scores in low noise levels, but they go through a sharp decrease when noise level increases. The reason is that strong noise extremely distracts the detectors, which results in locating an increasing number of discursive features. DoG detector, as expected, is robust to noise, but stays a lower repeatability than our detectors.

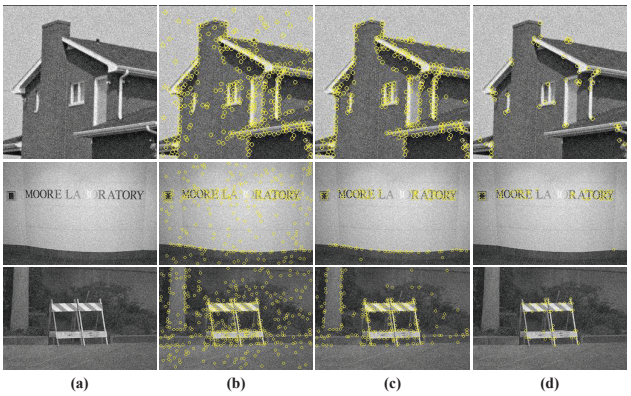

Figure 6: Detection results at different stages. (a) Original noisy images. (b) GDOBR result. (c) After rejecting features in flat regions. (d) After rejecting features on edge structures using an adaptive threshold. Noise with standard deviation 15 is added to the images.

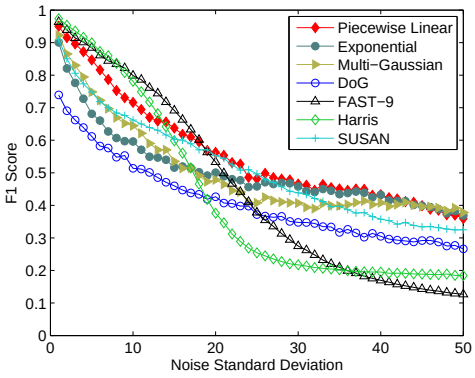

Figure 7: Average *F1* scores for images under different noise levels.

SUSAN approach, although has a higher *F1* score than DoG detector through noise, detects numerous edge based features, which are not stable in noise and also less discriminative. In contrast, our detectors have a better stability through different noise levels, and yield a higher *F1* score than other detectors in images with noise of high levels. This stability comes from the adaptive threshold for Harris response in our detection approach, which ensures the repeatability of the corners detected in images under different noise levels.

Among our three detectors, the detector built up with the piecewise linear function performs best. Lower scores are presented by the other two detectors when detecting corners in low noise level images. The reason is that the corners detected in noise-free images are the baseline for evaluating corners detected in noisy images, and the detector using the piecewise linear function could locate more accurate corners in noise-free images than the other two detectors. Therefore, a slight difference of the three fitting curves in high SNR values (above 25dB) shows a big difference in *F1* score, which can be observed in Fig. 5. Our detector adopts the piecewise linear function, for its good performance and simplicity. The detector is robust to noise as DoG, but yields a much higher repeatability.

Function	Formation	Parameters for best fitting	RMSE
Exponential	$f(x) = ae^{-bx}$	a = 8.376, b = 0.148	0.5264
Multi-Gaussian	$f(x) = a_1 e^{-(\frac{x-b_1}{c_1})^2} + a_2 e^{-(\frac{x-b_2}{c_2})^2}$	a_1 = 0.823, a_2 = 1.352×10^{12} b_1 = 10.36, b_2 = -310 c_1 = 5.926, c_2 = 60.73	0.5092
Piecewise Linear	$f(x) = \begin{cases} a_1x + b_1, & 0 < x < c_1 \\ a_2x + b_2, & c_1 \leq x \leq c_2 \\ a_3x + b_3, & x > c_2 \end{cases}$	a_1 = -0.207, b_1 = 4.059 a_2 = -0.044, b_2 = 1.201 a_3 = 0, b_3 = 0.05 c_1 = 17.53, c_2 = 26.13	0.5084

Table II: Formations of the three fitting functions and the parameters of the best fittings. We use two kernels for Gaussian function and three pieces for linear function.

V. Conclusions

In this paper, we have presented a corner detector which could locate discriminative corners in images under different noise levels. A modification to SUSAN principle enables our candidate corner detector to locate accurate corners in noise-free images efficiently. Based on the intensity centroid and the Harris response of the features, false corners detected in noise could be removed. Compared to some widely used point feature detectors, our detector could locate more discriminative and repeatable corners even in strong noise, which is attributed to the automatic image SNR estimation to refine features in noise. Since very few corner detectors is designed for noise invariance, we hope this work gives heuristic thoughts for noise-adaptive detection approaches. Our future work will focus on the noise robustness of point feature descriptors.

Acknowledgment

This work is supported by National Natural Foundation of China (Grant No. 61175032, 61302154, and 61304096).

References

[1] D. G. Lowe, "Distinctive image features from scale-invariant keypoints," *International Journal of Computer Vision*, vol. 60, no. 2, pp. 91–110, 2004.

[2] W. Zhao and C. Ngo, "Flip-invariant SIFT for copy and object detection," *IEEE Transactions on Image Processing*, vol. 22, no. 3, pp. 980–991, 2013.

[3] W. He, T. Yamashita, H. Lu, and S. Lao, "Surf tracking," in *IEEE International Conference on Computer Vision*, 2009, pp. 1586–1592.

[4] K. Mikolajczyk and C. Schmid, "Indexing based on scale invariant interest points," in *IEEE International Conference on Computer Vision*, vol. 1, 2001, pp. 525–531.

[5] J. Nakamura, *Image Sensors and Signal Processing for Digital Still Cameras*. Taylor & Francis Group, 2006, pp. 66–77.

[6] C. Harris and M. Stephens, "A combined corner and edge detector," in *Alvey vision conference*, vol. 15, 1988, pp. 147–151.

[7] S. M. Smith and J. M. Brady, "SUSAN – A new approach to low level image processing," *International Journal of Computer Vision*, vol. 23, no. 1, pp. 45–78, 1997.

[8] E. Rosten, R. Porter, and T. Drummond, "Faster and better: A machine learning approach to corner detection," *IEEE Trans. on Pattern Analysis and Machine Intelligence*, vol. 32, no. 1, pp. 105–119, 2010.

[9] O. A. Ahmed, "New denoising scheme for magnetic resonance spectroscopy signals," *IEEE Transactions on Medical Imaging*, vol. 24, no. 6, pp. 809–816, 2005.

[10] Y. Zhang, M. Brady, and S. Smith, "Segmentation of brain MR images through a hidden Markov random field model and the expectation-maximization algorithm," *IEEE Transactions on Medical Imaging*, vol. 20, no. 1, pp. 45–57, 2001.

[11] G. K. Rohde, A. S. Barnett, P. J. Basser, and C. Pierpaoli, "Estimating intensity variance due to noise in registered images: Applications to diffusion tensor MRI," *Neuroimage*, vol. 26, no. 3, pp. 673–684, 2005.

[12] S. Pyatykh, J. Hesser, and L. Zheng, "Image noise level estimation by principal component analysis," *IEEE Transactions on Image Processing*, vol. 22, no. 2, pp. 687–699, 2013.

[13] D. Zoran and Y. Weiss, "Scale invariance and noise in natural images," in *IEEE International Conference on Computer Vision*, 2009, pp. 2209–2216.

[14] J. T. L. Thong, K. S. Sim, and J. C. H. Phang, "Single-image signal-to-noise ratio estimation," *Scanning*, vol. 23, no. 5, pp. 328–336, 2001.

[15] J. Frank and L. Al-Ali, "Signal-to-noise ratio of electron micrographs obtained by cross correlation," *Nature*, vol. 256, pp. 376–379, 1975.

[16] M. Zou, *Deconvolution and Signal Recovery*. Beijing: National Defence Industry Press, 2001, pp. 184–189.

[17] C. Zhu, S. Li, Y. Song, and H. Chang, "Corner detector using invariant analysis," in *Proc. SPIE 8878, 5th International Conference on Digital Image Processing*, 2013.

[18] P. L. Rosin, "Measuring corner properties," *Computer Vision and Image Understanding*, vol. 73, no. 2, pp. 291–307, 1999.

[19] M. Weber, "Caltech background image dataset, http://www.vision.caltech.edu/html-files/archive.html."

[20] S. M. Smith, "http://users.fmrib.ox.ac.uk/˜steve/susan/ susan2l.c," 2005.